NANO LETTERS

pubs.acs.org/NanoLett
Letter

Molecular Dynamics Simulations Elucidate the Molecular Organization of Poly(beta-amino ester) Based Polyplexes for siRNA Delivery

Katharina M. Steinegger, Lars Allmendinger, Sebastian Sturm, Felix Sieber-Schäfer, Adrian P. E. Kromer, Knut Müller-Caspary, Benjamin Winkeljann, and Olivia M. Merkel*

Cite This: *Nano Lett.* 2024, 24, 15683−15692

ABSTRACT: Cationic polymers are known to efficiently deliver nucleic acids to target cells by encapsulating the cargo into nanoparticles. However, the molecular organization of these nanoparticles is often not fully explored. Yet, this information is crucial to understand complex particle systems and the role influencing factors play at later stages of drug development. Coarse-grained molecular dynamics (CG-MD) enables modeling of systems that are the size of real nanoparticles, providing meaningful insights into molecular interactions between polymers and nucleic acids. Herein, the particle assembly of variations of an amphiphilic poly(beta-amino ester) (PBAE) with siRNA was simulated to investigate the influence of factors such as polymer lipophilicity and buffer conditions on the nanoparticle structure. Simulations were validated by wet lab methods including nuclear magnetic resonance (NMR) and align well with experimental findings. Therefore, this work emphasizes that CG-MD simulations can provide underlying explanations of experimentally observed nanoparticle properties by visualizing the nanoscale structure of polyplexes.

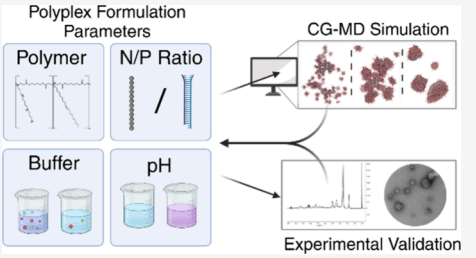

KEYWORDS: *Martini 3, RNA interference, polymers, polyplex*

Short-interfering ribonucleic acid (siRNA) as a therapeutic agent successfully entered the pharmaceutical market in 2018, with five FDA-approved products currently available.[1] Its mode of action is downregulation of transcription of disease driving genes via the mechanism of RNA interference (RNAi) in the target cells. However, while the demand for nucleic acid therapies is growing, all presently approved siRNA drugs target the liver.[2−5] A major challenge therefore remains in finding delivery vectors[6] which enable efficient targeting to other organs and simultaneously avoid early degradation of the RNA.

The five marketed siRNA therapies rely either on lipid nanoparticles (LNPs) or conjugation to trivalent *N*-acetylgalactosamine (GalNAc) to ensure delivery.[1] Besides viral vectors, alternatives for delivery vehicles include polymers. Cationic polymers encapsulate the negatively charged RNA mainly via electrostatic interactions,[7] forming so-called poly- or micelleplexes. Using polymers as delivery vectors provides certain advantages,[8,9] such as broad tunability and good biodegradability. Therefore, polycations are being investigated as nonviral vectors for safe and efficient delivery targeting a wide variety of diseases.[10−13] The explored materials cover a broad chemical space ranging from polyethylenimines (PEI),[14,15] via carbohydrates such as chitosan,[16] to more complex molecular structures such as poly(beta-amino ester)s (PBAEs).[17]

PBAEs were first introduced as polycationic vectors for plasmid DNA in the year 2000[18] and stand out due to their almost unlimited adaptability. Owing to a toolbox-like system, PBAEs allow various combinations of diacrylates for the backbone and amines as side chains of the molecular structure.[19] The introduction of amphiphilicity by combination of hydrophilic and hydrophobic side chains within one polymer was shown to improve colloidal stability.[20] Subsequently, amphiphilic PBAEs, containing a varying ratio of polycationic spermine and lipophilic oleylamine (OA), have been identified as copolymers that successfully deliver siRNA, achieving particularly high knockdown efficiencies at low polymer-to-RNA ratios.[21]

Understanding the internal organization of self-assembled polyplexes can help to identify relevant formulation parameters and to link these to the particles' physicochemical properties.[7] Subsequently, the intracellular behavior of polyplexes can further be elucidated.[22,23] Experimental methods including transmission electron microscopy (TEM)[7,24] or small-angle X-ray scattering (SAXS)[25] have been applied to investigate particle shapes. Others have exposed the role of the molecular

Received: September 2, 2024
Revised: November 1, 2024
Accepted: November 4, 2024
Published: November 26, 2024

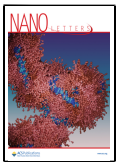

https://doi.org/10.1021/acs.nanolett.4c04291
Nano Lett. 2024, 24, 15683−15692

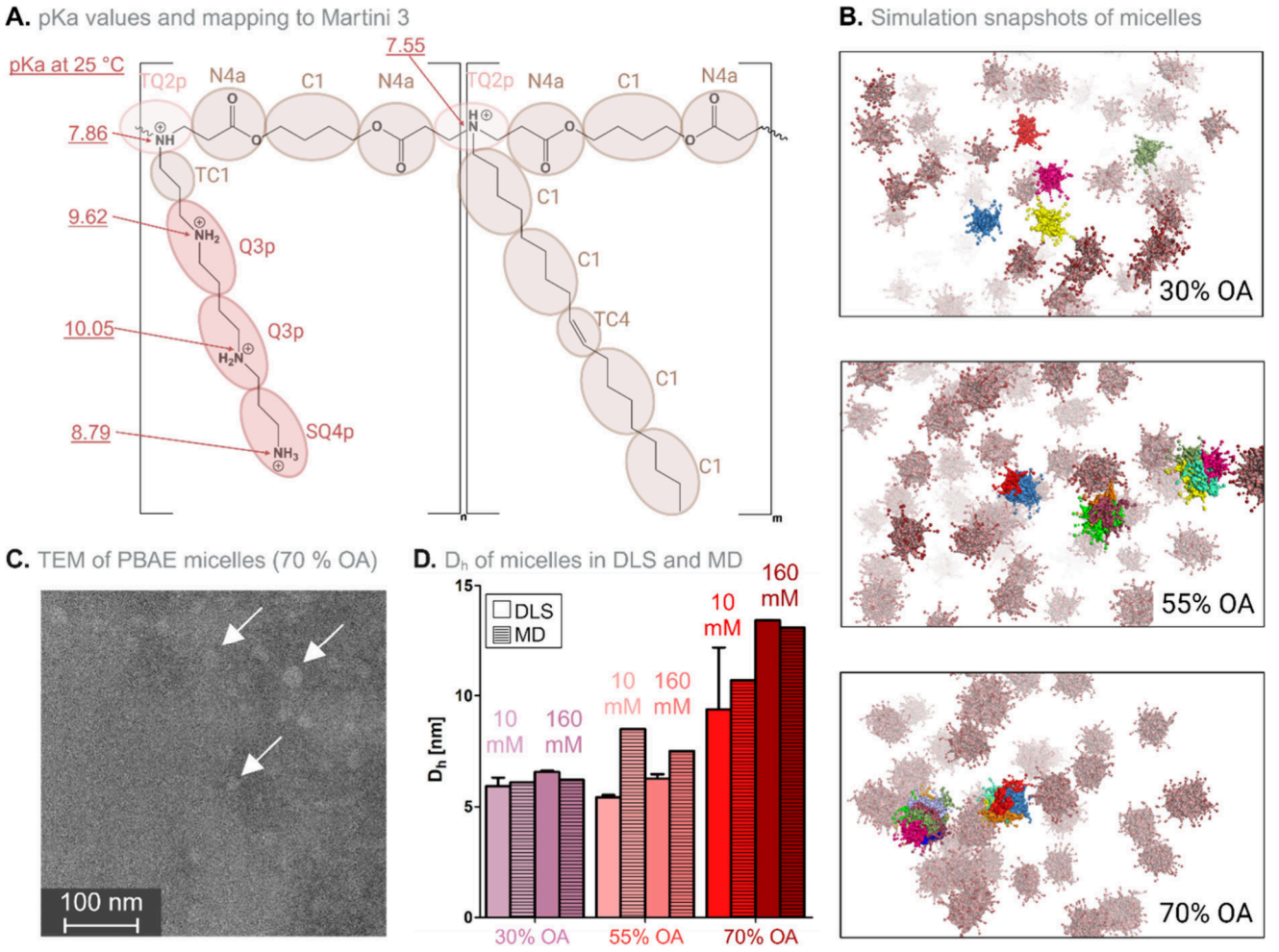

Figure 1. PBAE mapping and model validation. (A) Molecular structure and pK_a values at 25 °C of the PBAE copolymer with spermine (left) and oleylamine (right) subunit. Mapping to CG resolution within Martini 3 indicated by spheres. (B) Simulation snapshots of 9 kDa polymers in 10 mM HEPES at pH 5.4, simulated for 2.5 μs. Lipophilic components in gray, charged beads in red. Exemplary coloring corresponds to one polymer molecule per color. (C) Micelles formed of PBAE 70% OA as visible in TEM imaging. (D) Comparison of hydrodynamic diameters in DLS and simulation (MD) under low and high ionic strength buffer conditions. DLS results (n = 3) with mean ± SD of main peak below 20 nm by intensity. MD results are the mean of D_h averaged over the whole box, calculated from mean square deviation (msd) between 1.75 and 2.25 μs of simulated time.

weight (MW) of PBAEs by explicitly screening its influence on knockdown efficiency.[26] Meanwhile, molecular dynamics (MD) simulations have developed into a powerful tool to be incorporated in the development of drug delivery systems.[27−29] Especially with the refinement of coarse-grained (CG) models, MD allows for simulating systems in the size of real nanoparticles up to 100 nm at time scales of several microseconds.[30,31]

Herein, PBAEs comprising spermine as a polycationic moiety and OA as a lipophilic component, have been mapped and parametrized in CG resolution in the Martini 3 force field.[32] The parametrization, based on the mapping (Figure 1A), yielded distributions of bonded interactions in good agreement with the all-atom (AA) reference (Figure S1A,B). The herein studied PBAE polyplexes are exposed to an acidic pH of 5.4 during polyplex formulation, a pH of 7.4 upon administration, and again acidic pH after cellular internalization in the endosomal compartment.[22] According to the pK_a values determined by density functional theory (DFT), all amines of the polymer were protonated at pH 5.4. At pH 7.4, only the secondary amines and the tertiary amine of the OA linkage in the backbone were protonated (Figure 1A). The remaining amines in the spermine moiety were considered deprotonated due to neighboring effects of the protonated secondary amines (Figure S2). PBAE models were generated for polymers with varying % OA between 10% and 85%. Initially, a MW of approximately 9 kDa was chosen. To account for possible influences of the MW, models with 4.5, 27, and 100 kDa were generated additionally. As the behavior of these models showed no notable differences upon particle formation in visible outputs and radial distribution functions (RDF) around RNA phosphates (Figure S3), further simulations were conducted with the 9 kDa models. Micelle formation of the amphiphilic polymer (Figure 1B) was confirmed by TEM imaging (Figure 1C), dynamic light scattering (DLS) (Figure 1D), and a pyrene assay for the critical micellar concentration (CMC) (Figure S4), with decreasing CMCs observed as the % OA increased.

To validate the behavior of the polymer models, setups with only PBAE in buffer were simulated, and the average hydrodynamic diameter of micelles was calculated via mean square deviation (msd). The micelle sizes in simulation were in

https://doi.org/10.1021/acs.nanolett.4c04291
Nano Lett. 2024, 24, 15683−15692

good agreement with DLS results (Figure 1D) and followed the trend of increasing micelle size with increasing % OA of the polymer. Analysis of TEM images yielded a diameter of 18.8 ± 3.8 nm for the 70% OA polymer in 10 mM HEPES, which is larger than those of DLS (9.4 ± 2.8 nm) and simulation (10.7 nm). This deviation was attributed to the increased visibility of larger micelles in the TEM and unclear margins of the single micelles. Another explanation can be an increased sample concentration in TEM making the formation of larger polymer aggregates more favorable, especially considering the high lipophilicity of the 70% OA polymer.

Previous *in vitro* experiments with this type of PBAE copolymer,[21] and other PBAE-based studies[33] showed a strong influence of the polymers' amphiphilicity on knockdown or transfection efficiency. Hence, the % OA in the polymer was selected as a factor for an in-depth *in silico* investigation. Upon simulation of particle assembly, precursor micelles assembled within the first μs. Polycationic spermine moieties remained on the surface and established electrostatic interactions with the negatively charged phosphate beads of siRNA (Figure 2A).

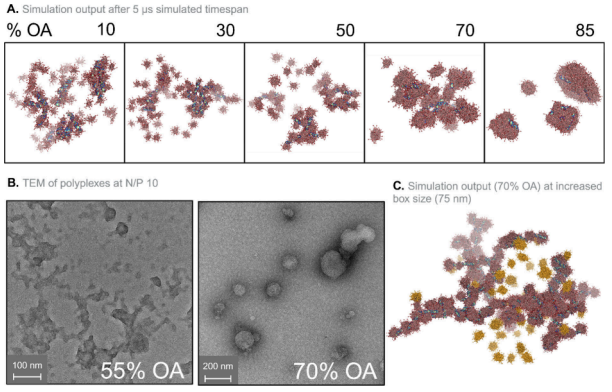

Figure 2. Influence of polymer lipophilicity on particle morphology (in 10 mM HEPES, pH 5.4, at N/P 10). (A) Simulation output after 5 μs of particle assembly with increasing lipophilicity, i.e., % OA of the polymer (10%, 30%, 50%, 70%, and 85% shown) from left to right. Polymers in gray/red, siRNA in turquoise. (B) Particles formed with either 55% or 70% OA in TEM. (C) Simulation output of particle assembly under the same conditions as in (A) for 70% OA but in a cubic box with 75 nm side length, containing 99 siRNA molecules. Orange color represents the polymer outside of siRNA containing particles.

Over time, this led to the formation of nanoparticles. Unlike for the micelles, the particle sizes cannot be directly compared between simulation and experiment, as the simulation box does not contain enough material to form real sized nanoparticles.

Zhao et al.[34] demonstrated in an AA simulation setup the exclusive interaction of spermines with the major groove of siRNA. Notably, this exclusivity of interaction was not reproduced in our model (Figure S5), which could be attributed to the reduced mobility of the spermines anchored in the PBAE backbone at GC resolution. Shortcomings of the Martini 3 force field, including nonideal nonbonded interactions,[35] have been reported. Therefore, detailed small-scale interactions profit from the application of an AA simulation, whereas CG-MD is advantageous for large-scale simulation setups due to the massive reduction of consumed resources.

The particle morphology was strongly influenced by the lipophilicity of the copolymer: Low % OA polymers formed undefined particles with rugged surfaces. Increasing the % OA led to irregular, "bead-on-a-string"-like particles, as previously described for other polyplexes.[7,24] Only above 70% OA, compact particles formed (Figure 2A). TEM images (Figure 2B) confirmed a change in particle shape with 55% OA polymer particles being irregularly shaped and 70% OA polymer particles appearing condensed. The differences in particle shape between MD and TEM in the range from 70 to 80% OA might be attributed to the limited time of assembly during the simulations. The 70% OA, N/P 10 (ratio of PBAE-amines to RNA phosphates) particle assembly was therefore extended to 15 μs. However, the particle only slightly condensed further but did not reach a similarly compacted shape, as observed in the corresponding TEM images (Figure S6). As particle assembly in wet lab experiments requires incubation times in the minute range, the process could be too slow to be portrayed in simulation to the final state. To determine if the limited simulation size of the cubic 40 nm box affects particle assembly, the 70% OA polymer was exemplarily simulated in a 75 nm box with 99 siRNA molecules (Figure 2C). The RDF around RNA phosphates showed similar contact levels with amines and water (Figure S7) compared to those of the smaller setup, validating the use of the 40 nm box simulations.

The trends in particle shape were attributed to the capability of different polymers to form larger supramolecular assemblies, i.e., elongated micellar structures, spheres with RNA containing pores, or larger micelles in general. With increasing % OA, the total mass of polymer to achieve the same N/P ratio increases, as the number of charged spermines within the same total mass of polymer decreases. In the simulations, this was quantified as the number of spermines per nm^2 of the micelle core surface (Figure S8). With increasing % OA, the spermine density on the micelle surface decreased; therefore, the repulsion between single micelles was reduced. Thus, larger polymer arrangements formed, and more compacted particle shapes were accessible.

The N/P ratio is often correlated with the knockdown efficiency of siRNA polyplexes[7] and was shown to be of high impact for the characteristics of particles formed with the PBAEs.[21] Here, nanoparticles were prepared for polymers with 30%, 55%, and 70% OA at N/P ratios 1−10 and the polymers' encapsulation efficiencies were assessed. Z-average and PDI (Figure S9A) confirmed the formation of small (<100 nm) and monodisperse (PDI < 0.2) nanoparticles for all polymers within an optimized N/P range. The ζ-potential increased with increasing N/P ratio from below 0 mV to maximum values around 20 mV. All formulations benefited from an N/P ratio where the ζ-potential (Figure S9B) was positive. In contrast, in the N/P range around charge neutrality, standard deviations for Z-average and PDI were high due to aggregation tendencies of the nanoparticles. The PDI was lowest just above charge neutrality and increased with the addition of more polymer, arguably due to the formation of excess micelles as a second species. This indicated an optimal N/P ratio of 5−6 for the 30% and 55% OA polymers, while the 70% OA polymer formed the smallest and most monodisperse particles at N/P 7−10. This observation corresponds well with the N/P values at which full encapsulation was reached: Figure 3A shows that for 30% and 55% OA, full encapsulation was achieved at N/P ≈ 4, with no notable difference between the two polymers. The more lipophilic polymer (70% OA) reached full encapsulation at a N/P ratio of around 6.

https://doi.org/10.1021/acs.nanolett.4c04291
Nano Lett. 2024, 24, 15683−15692

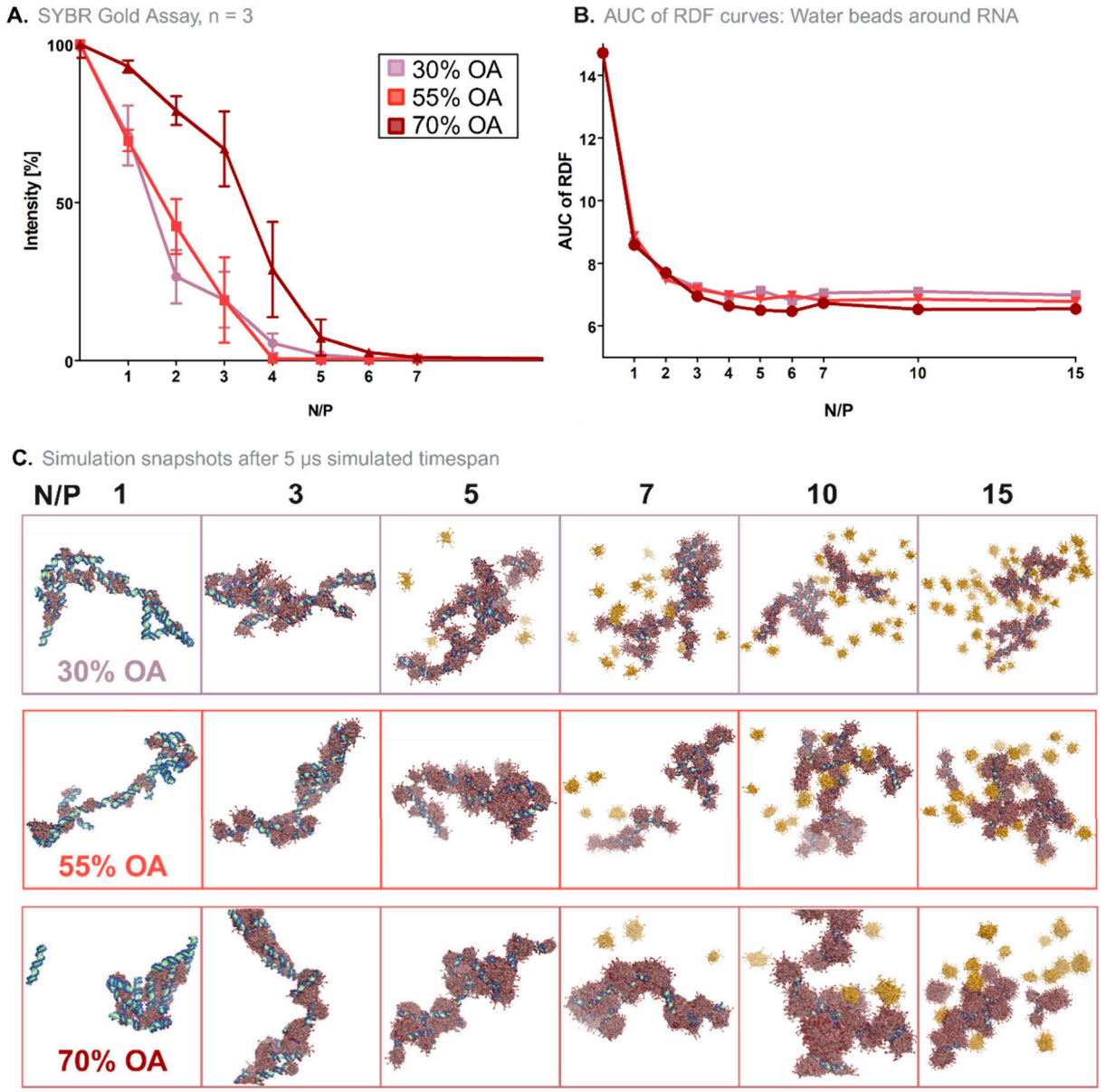

Figure 3. Nanoparticles at different N/P ratios. (A) Encapsulation efficiency experimentally assessed by the SYBR Gold assay, n = 3, shown as mean ± SD. (B) Area under the curve (AUC) of radial distribution functions (RDF) within 0.6 nm of the RNA surface, indicating the decrease of water contacts of the RNA with increasing N/P ratios. (C) Simulation output after 5 μs simulated particle assembly with increasing N/P ratios from left to right, simulated with 30%, 55%, and 70% OA polymers. Excess polymer (outside of RNA containing particles) is shown in orange.

Subsequently, MD simulations were conducted with the same polymers at N/P ratios from 1 to 15. The encapsulation efficiency within the simulations was quantified via the area under the curve (AUC) of the RDF for the water contacts of the RNA surface (Figure S10). Figure 3B shows a decrease of water contacts until N/P 4 is reached for all polymers, which fully corroborates the experimental results for 30% and 55% OA. Conversely, the difference of encapsulation efficiency for the 70% OA polymer between N/P 1−5 was not reproduced. As observed with the results for particle morphology, this suggests inaccuracies of the CG-MD approach in the middle to high % OA range.

It was, however, visible in the simulation output that particles formed by the hydrophilic polymers (30% and 55% OA) contained more spermine moieties on the particle surface at low N/P ratios (Figure 3C, N/P 3 and 5). These spermines were not in reach of any RNA backbone and therefore did not contribute to RNA complexation. Instead, they formed a charged corona on the particle surface. The simulations thus provide an explanation for the transition from negative to positive ζ-potential at lower N/P ratios for particles with lower % OA PBAEs. Again, the observed effect can be attributed to limited possibilities for the supramolecular arrangement of the polymer within the smaller micelles.[29]

Further, the choice of N/P ratio is of high relevance as an excess of unnecessary excipients can promote side effects.[36−38] Figure 3C shows the first appearance of free, excess polymer at N/P 5 for 30% OA and N/P 7 for 55% and 70% OA. The amount of free polymer and, from that, the stoichiometry (i.e., effective N/P ratio) in MD simulations was quantified for all polymer models between 10% and 85% OA at N/P 10 in different buffers (Figure 4A). The trend clearly suggests that

https://doi.org/10.1021/acs.nanolett.4c04291
Nano Lett. 2024, 24, 15683−15692

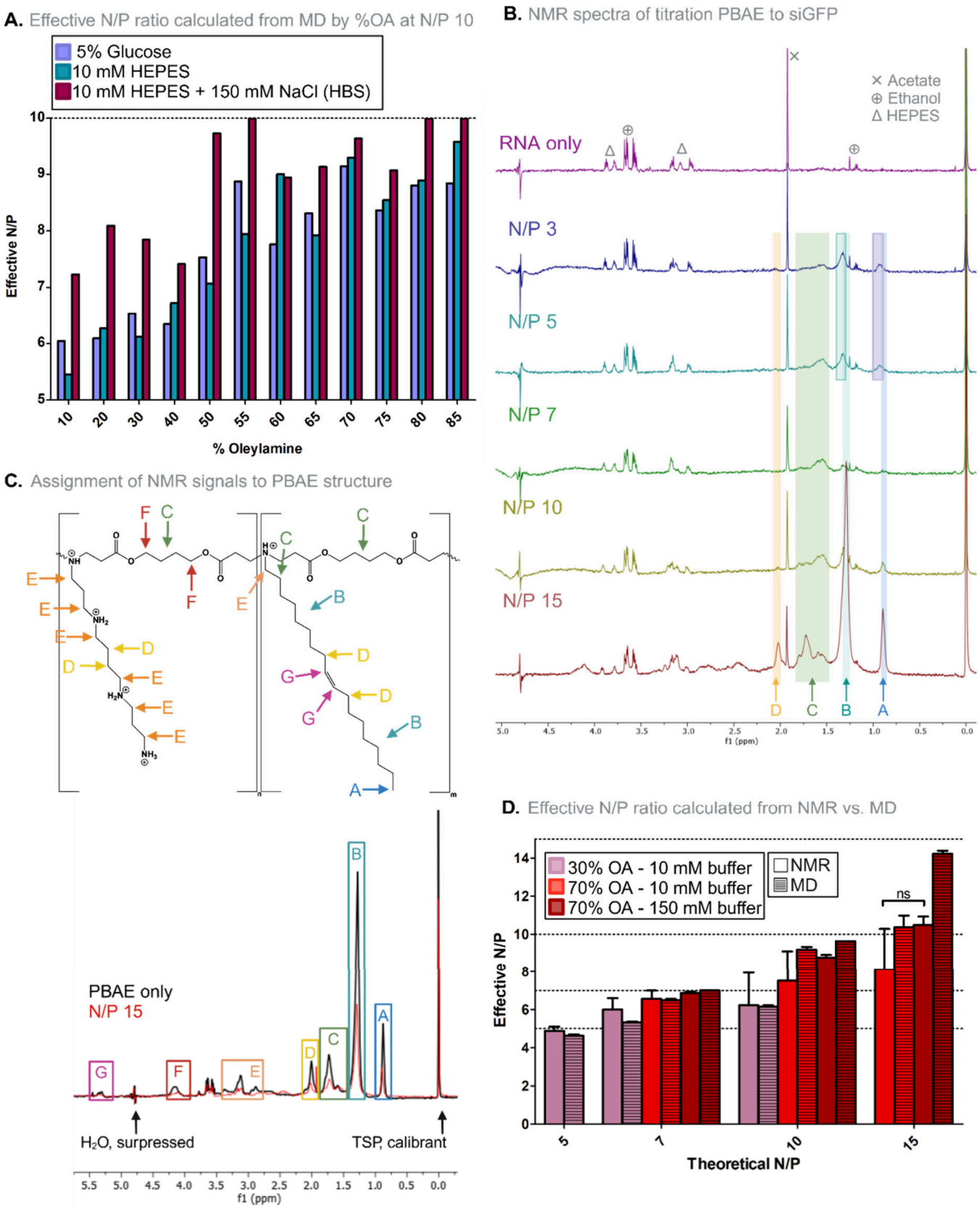

Figure 4. Simulation validation by NMR. (A) Effective N/P ratio calculated from MD (n = 1) at an input N/P ratio of 10. Simulated for polymers from 10% to 85% OA in 5% glucose, 10 mM HEPES or 10 mM HEPES + 150 mM NaCl (= HBS). (B) ^{1}H NMR spectra with water suppression (10 mM PBS, pH 5.4, and 10% D_2O/H_2O). N/P ratios increase from top to bottom by stepwise addition of 70% OA polymer to the sample. Signals with the most prominent changes upon titration are marked by boxes. (C) Excerpt of chemical structure of PBAE, signal assignment, and overlay of ^{1}H NMR spectra of N/P 15 and PBAE only; NMR conditions as described under A. (D) Effective N/P ratio calculated from NMR (n = 3, mean ± SD) in comparison to MD (n = 2, mean).

https://doi.org/10.1021/acs.nanolett.4c04291
Nano Lett. 2024, 24, 15683−15692

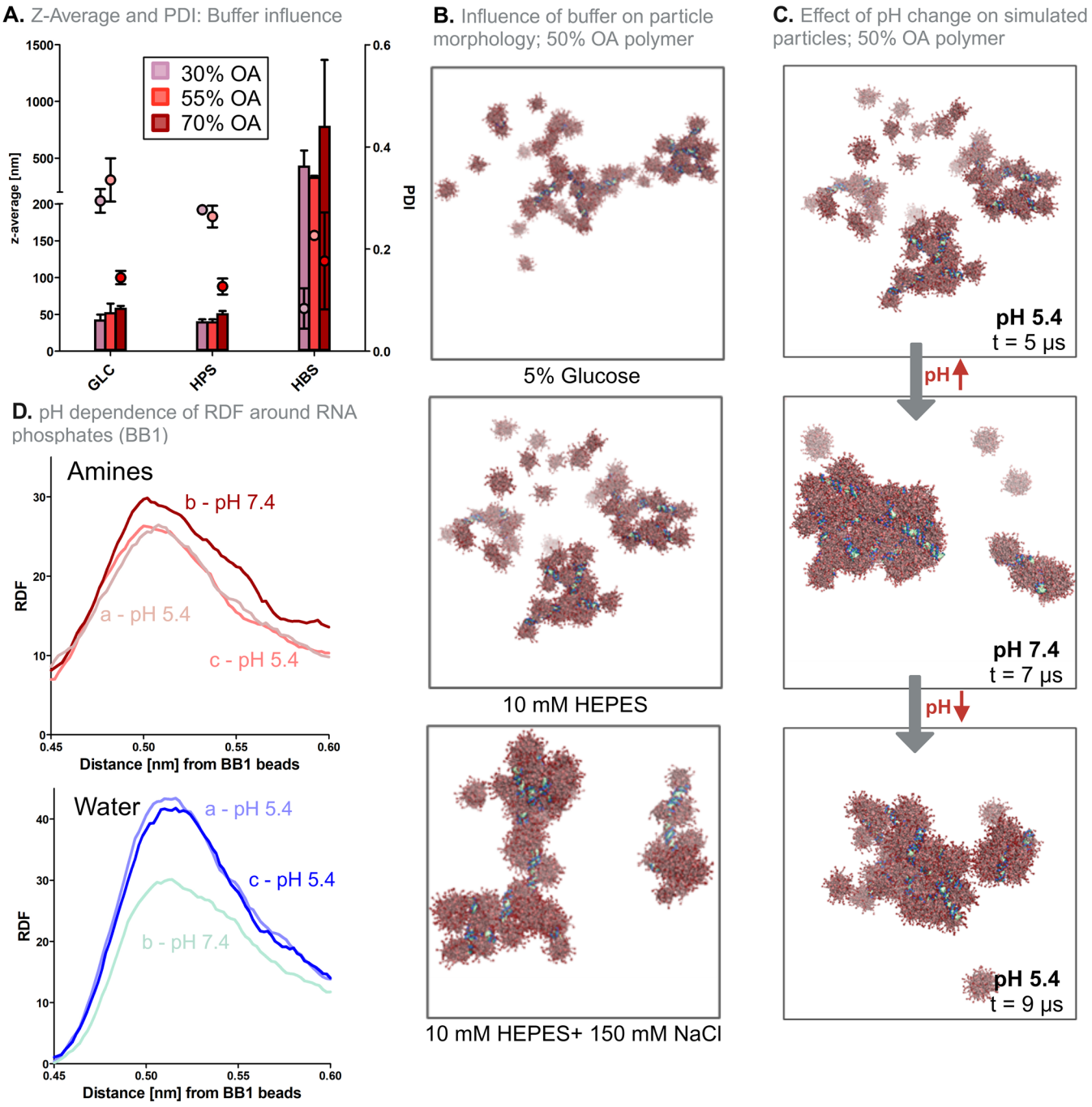

Figure 5. Influence of buffer conditions on PBAE polyplexes. (A) Z-average (bars) and PDI (dots) of polyplexes at N/*P* = 10 in 5% glucose, 10 mM HEPES or 10 mM HEPES + 150 mM NaCl (= 160 mM HBS), all pH 5.4. *n* = 3, mean ± SD. (B) Last frame of simulated particle assembly (5 *μs*) in different buffers. (C) Visualization of changes in particle structure after simulation of subsequent pH changes (assembly at pH 5.4 for 5 *μs*, equilibration at pH 7.4 for 2 *μs*, and equilibration back to pH 5.4 for 2 *μs*). (D) RDF of amines of 50% OA PBAE (top) and water (bottom) around RNA phosphate beads after initial particle assembly, after pH increase to pH 7.4, and after subsequent reduction of the pH back to 5.4.

the more lipophilic the polymer, the higher the amount polymer bound per siRNA, leading to higher effective N/P ratios.

These simulation results were validated by ^{1}H nuclear magnetic resonance (NMR) spectroscopy. By titration of an siRNA sample with increasing amounts of PBAE and measurement of an ^{1}H NMR spectrum after each step, new signals referring to excess polymer were identified above certain N/P ratios (Figure 4B). After the addition of the first PBAE to siRNA, additional signals appeared incrementally. Assuming that the polyplex signals are not visible due to severe line broadening resulting from short transverse relaxation times (T_2), these signals were attributed to dangling residues on the polyplex surface.[39] In comparison to the peaks of PBAE only samples and samples with high N/P, these signals are slightly shifted toward higher ppm. At high N/P ratios, the most prominent signals showing a constant increase in intensity were signals A, B, C, and D (Figure 4B,C). Signals A and B can be exclusively attributed to the OA[40,41] within the polymer (Figure S11).

https://doi.org/10.1021/acs.nanolett.4c04291
Nano Lett. 2024, 24, 15683−15692

The appearance of the free polymer at high N/P ratios was confirmed by 2D NOESY experiments. These are based on the nuclear Overhauser effect (NOE), used to detect spatial proximity of protons/the chemical exchange of protons in different chemical environments.[42,43] This type of experiment was performed with samples containing RNA and 70% OA polymer at N/P = 7 or 15 (Figure S12). First, reference spectra containing only PBAE were analyzed. Very intense intramolecular NOEs are present, mainly originating from the OA moiety of the polymer. At an N/P ratio of 7, all intramolecular NOEs nearly collapse or are not visible at all due to the extreme line broadening. This may be due to either the sole presence of a giant supramolecular assembly i.e., polyplexes with low tumbling rates leading to drastically increased transverse relaxation rates (R_2), or transitions between free and bound states with significantly different chemical shifts in the slow intermediated exchange regime on the NMR time scale.[44] These findings are in good agreement with the *in silico* results, indicating that an N/P ratio around 7 represents a stoichiometric inflection point in polyplex formation with 70% OA PBAE. Finally, if a relatively large excess of polymer is obtained (N/P 15), the NOEs previously present in the reference spectrum (PBAE only) become visible again.

Both methods (NMR and CG-MD) implied that the stoichiometry within the particles no longer increased linearly with the theoretical N/P ratio (Table S1 and Figure S13). Instead, the effective N/P ratio in 10 mM phosphate buffered saline (PBS) reached a threshold of about 9 for 70% OA polyplexes and about 6 for the 30% OA PBAE particles.

The good agreement between NMR results and effective N/P ratios from the MD simulations (Figure 4D) highlights the accuracy of the MD model. The strongest deviation between NMR and MD results was measured in high ionic strength buffer (150 mM PBS in NMR or 160 mM HEPES buffered saline (HBS) in MD) at an input N/P ratio of 15. Here, MD results imply nearly full binding of the 70% OA polymer. This trend toward higher effective N/P ratios in high ionic strength buffers was consistent throughout all simulations (Figure 4A). However, by NMR no significant difference was observed at N/P = 15 between particles formed in high or low ionic strength buffer with 70% OA PBAE (Figure 4D).

Notably, concentrations in MD simulations were about 100× higher than in experimental setups, which might have contributed to the observed deviation between the NMR and MD results. Additionally, the reaction field (rf) algorithm used to handle electrostatic interactions in the MD setup comprises a trade-off with improved computational performance but reduced accuracy of the simulation, as it uses a coulomb cutoff beyond which the dielectric constant of the system is treated as uniform.[45] This leads to poorer treatment of long-range electrostatics in comparison to e.g., the Particle Mesh Ewald algorithm (PME).[46] Still, ionic strength of the medium is known to often influence colloidal stability and size of nanoparticles[47,48] and will therefore be further discussed below.

To determine the influence of buffer excipients, particles were formulated at N/P 10 in three different buffers/solutions at pH 5.4: 5% glucose, 10 mM HEPES, and 160 mM HBS. DLS measurements revealed a shift toward larger particles (Figure 5A) with a higher ζ-potential (Figure S14) at a high ionic strength of the medium, independent of the lipophilicity of the used polymer. Although no significant difference between 5% glucose and 10 mM HEPES concerning size and ζ-potential was observed, the presence of ions at higher concentrations (HBS) caused significantly larger particles with hydrodynamic diameters of above 400 nm. In MD simulation, visually more compact particles formed (Figure 5B), and, as discussed above, the effect of ionic strength resulted in higher effective N/P ratios.

The presence of more ions in the hydrodynamic shell of the PBAE micelles alters the repulsive forces upon particle assembly. Reduced colloidal stability and altered particle shapes are therefore to be expected. Furthermore, surface charge of nanoparticles is known to alter their interaction in physiological environments e.g., with proteins in serum.[49] Ultimately, this influences cellular uptake and intracellular trafficking.[50−52]

When the particle contains functional groups with pK_a values in physiological ranges, pH changes in the surrounding medium will alter the particle charge and its interactions with the environment.[53] To mimic these changes in the simulation, pH values of 5.4 (formulation), followed by pH 7.4 (administration), and again pH 5.4 (endosome) were applied via an adjustment of the protonation state of the polymer.[31] Increasing the pH to 7.4 caused condensation of the particles as the decreased charge on the micelle surface allowed for a rearrangement of the micelles into larger supramolecular structures (Figure 5C). These changes reduced the number of water contacts of the RNA phosphates (Figure 5D) but increased the number of contacts with amines. In contrast to CG-MD observations made on lipid-based RNA carriers,[31] the pH increase did not cause expulsion of RNA from the particle. After the pH was reduced again, the particles rearranged but primarily maintained their agglomerated shape. However, the microenvironment around the phosphates restored to the level as before the pH changes, for both water and amine contacts. Especially for high % OA particles, the shapes resulting after the pH changes align better with the TEM images (Figure 2B, Figure S6) than before. It could therefore be argued that the pH changes speed up the process of particle condensation, which is otherwise too slow to simulate a final state. The readjustment to pH 5.4 was accompanied by a moderate swelling of the polyplex, which was hypothesized previously to play a role in endosomal escape.[50]

With a combinatorial approach of CG-MD simulation and experimental validation, experimentally observed influences on the polyplex structure were explained on a molecular level. Our CG-MD approach did not suggest a pronounced effect of MW of the polymer for the investigated PBAEs. Instead, lipophilicity of the PBAE was identified to be the main influencing factor on particle shape, reflected by the charge, density, and mobility of spermines on the surface of polymeric micelles. Polyplex morphology may strongly affect cellular uptake and endosomal escape.[54] Hence, the demonstrated influence of the lipophilicity of the polymer should be carefully considered when designing amphiphilic PBAEs. Structural alterations of polyplexes were also observed through changes in pH and ionic strength of the medium. Furthermore, with CG-MD and NMR, two methods were introduced to determine the critical N/P_{max} for every % OA. Further increasing the N/P in the formulation did not significantly increase the stoichiometry within the particles. PBAEs are a heterogeneous group of polymers, varying not only in lipophilicity but also, for example, backbone rigidity or side-chain architecture. Similar simulation setups could therefore be applied to other PBAE

https://doi.org/10.1021/acs.nanolett.4c04291
Nano Lett. 2024, 24, 15683−15692

structures, allowing for a more extensive comparison of the polymers.

Future work will have to show how the herein found differences between polyplexes of varying lipophilicity and structure are linked to their differing behavior *in vitro* and *in vivo*. A quantitative approach that directly links *in silico* data to *in vitro* data is however a major hurdle, as the simulation of whole cells, including their active mechanisms and pathways, is not possible yet.[55] Still, future simulations could provide underlying explanations for differences in biological interaction (e.g., endosomal escape).[23]

In this work, despite minor limitations in reproducing experimental results at high % OA, computational results were generally consistent with experimental findings. By comparing experiments with CG-MD simulations, this study clarifies the molecular organization of PBAE polyplexes and demonstrates the utility of CG-MD in the development of drug delivery systems.

■ ASSOCIATED CONTENT

Supporting Information

The Supporting Information is available free of charge at https://pubs.acs.org/doi/10.1021/acs.nanolett.4c04291.

> Additional simulation data (bonded distributions of the PBAE model and the HEPES model, visual simulation output of MW and simulation time comparisons, RDFs, spermine density on micelle cores plotted against % OA, viscosity results of simulated buffers/solvents), complete pK_a results from DFT, CMC results from pyrene assay, Z-averages with PDIs and ζ-potentials for 30%, 55%, and 70% OA nanoparticles, ζ-potential dependency on solvent/buffer, additional NMR results (proton assignment, 2D NOESY spectra, linear regressions for the analysis of free PBAE, tabulated effective N/P results), method descriptions for *in silico* experiments (DFT, CG-MD), wet lab experiments (polyplex formulation, pyrene assay, TEM, ^{1}H NMR, 2D NOESY), and data analysis (PDF)

■ AUTHOR INFORMATION

Corresponding Author

Olivia M. Merkel − *Department of Pharmacy, Ludwig-Maximilians-University Munich, 81377 Munich, Germany; Center for NanoScience (CeNS), Ludwig-Maximilians-University Munich, 80799 Munich, Germany; Comprehensive Pneumology Center Munich (CPC-M), Helmholtz Munich, 81377 Munich, Germany;* orcid.org/0000-0002-4151-3916; Email: olivia.merkel@lmu.de

Authors

Katharina M. Steinegger − *Department of Pharmacy, Ludwig-Maximilians-University Munich, 81377 Munich, Germany;* orcid.org/0009-0002-3396-9654

Lars Allmendinger − *Department of Pharmacy, Ludwig-Maximilians-University Munich, 81377 Munich, Germany*

Sebastian Sturm − *Department of Chemistry, Ludwig-Maximilians-University Munich, 81377 Munich, Germany; Center for NanoScience (CeNS), Ludwig-Maximilians-University Munich, 80799 Munich, Germany*

Felix Sieber-Schäfer − *Department of Pharmacy, Ludwig-Maximilians-University Munich, 81377 Munich, Germany*

Adrian P. E. Kromer − *Department of Pharmacy, Ludwig-Maximilians-University Munich, 81377 Munich, Germany*

Knut Müller-Caspary − *Department of Chemistry, Ludwig-Maximilians-University Munich, 81377 Munich, Germany; Center for NanoScience (CeNS), Ludwig-Maximilians-University Munich, 80799 Munich, Germany;* orcid.org/0000-0002-2588-7993

Benjamin Winkeljann − *Department of Pharmacy, Ludwig-Maximilians-University Munich, 81377 Munich, Germany; Center for NanoScience (CeNS), Ludwig-Maximilians-University Munich, 80799 Munich, Germany; Comprehensive Pneumology Center Munich (CPC-M), Helmholtz Munich, 81377 Munich, Germany;* orcid.org/0000-0002-6334-6696

Complete contact information is available at: https://pubs.acs.org/10.1021/acs.nanolett.4c04291

Notes

O.M. is a consultant for PARI Pharma GmbH and AbbVie Deutschland GmbH, and an advisory board members for AMW GmbH, Coriolis Pharma GmbH and Corden Pharma International GmbH on unrelated projects. O.M. and B.W. are cofounders of RNhale GmbH.

The authors declare no competing financial interest.

■ ACKNOWLEDGMENTS

O.M.M. acknowledges funding from the European Research Council (ERC-2022-COG-101088587). This work was supported through the Leibnitz Supercomputing Centre in the framework of the project AVOCADO - AdVanced fOrmulation using Coarse grAineD mOdelling to B.W. Additionally, we thank Jonas Binder for valuable input concerning the CG-MD work.

■ REFERENCES

(1) Traber, G. M.; Yu, A. M. RNAi-Based Therapeutics and Novel RNA Bioengineering Technologies. *J. Pharmacol Exp Ther* **2023**, *384* (1), 133−154.

(2) Kristen, A. V.; Ajroud-Driss, S.; Conceicao, I.; Gorevic, P.; Kyriakides, T.; Obici, L. Patisiran, an RNAi therapeutic for the treatment of hereditary transthyretin-mediated amyloidosis. *Neurodegener Dis Manag* **2019**, *9* (1), 5−23.

(3) Balwani, M.; Sardh, E.; Ventura, P.; Peiro, P. A.; Rees, D. C.; Stolzel, U.; Bissell, D. M.; Bonkovsky, H. L.; Windyga, J.; Anderson, K. E.; Parker, C.; Silver, S. M.; Keel, S. B.; Wang, J.-D.; Stein, P. E.; Harper, P.; Vassiliou, D.; Wang, B.; Phillips, J.; Ivanova, A.; Langendonk, J. G.; Kauppinen, R.; Minder, E.; Horie, Y.; Penz, C.; Chen, J.; Liu, S.; Ko, J. J.; Sweetser, M. T.; Garg, P.; Vaishnaw, A.; Kim, J. B.; Simon, A. R.; Gouya, L. Phase 3 Trial of RNAi Therapeutic Givosiran for Acute Intermittent Porphyria. *N. Engl J. Med.* **2020**, *382* (24), 2289−2301.

(4) Garrelfs, S. F.; Frishberg, Y.; Hulton, S. A.; Koren, M. J.; O'Riordan, W. D.; Cochat, P.; Deschenes, G.; Shasha-Lavsky, H.; Saland, J. M.; van't Hoff, W. G.; Fuster, D. G.; Magen, D.; Moochhala, S. H.; Schalk, G.; Simkova, E.; Groothoff, J. W.; Sas, D. J.; Meliambro, K. A.; Lu, J.; Sweetser, M. T.; Garg, P. P.; Vaishnaw, A. K.; Gansner, J. M.; McGregor, T. L.; Lieske, J. C. Lumasiran, an RNAi Therapeutic for Primary Hyperoxaluria Type 1. *N Engl J. Med.* **2021**, *384* (13), 1216−1226.

(5) Ray, K. K.; Wright, R. S.; Kallend, D.; Koenig, W.; Leiter, L. A.; Raal, F. J.; Bisch, J. A.; Richardson, T.; Jaros, M.; Wijngaard, P. L. J.; Kastelein, J. J. P. Orion; Investigators, O.-. Two Phase 3 Trials of Inclisiran in Patients with Elevated LDL Cholesterol. *N Engl J. Med.* **2020**, *382* (16), 1507−1519.

(6) Belgrad, J.; Fakih, H. H.; Khvorova, A. Nucleic Acid Therapeutics: Successes, Milestones, and Upcoming Innovation. *Nucleic Acid Ther* **2024**, *34* (2), 52−72.
(7) Zheng, M.; Pavan, G. M.; Neeb, M.; Schaper, A. K.; Danani, A.; Klebe, G.; Merkel, O. M.; Kissel, T. Targeting the blind spot of polycationic nanocarrier-based siRNA delivery. *ACS Nano* **2012**, *6* (11), 9447−54.
(8) Kavanagh, E. W.; Green, J. J. Toward Gene Transfer Nanoparticles as Therapeutics. *Adv. Healthc Mater.* **2022**, *11* (7), No. e2102145.
(9) Merkel, O. M.; Kissel, T. Quo vadis polyplex? *J. Controlled Release* **2014**, *190*, 415−23.
(10) Chu, Z.; Li, Z.; Yong, H.; Che, D.; Li, B.; Yan, C.; Zhou, T.; Wang, X.; Feng, Y.; Guo, K.; Geng, S. Enhanced gene transfection and induction of apoptosis in melanoma cells by branched poly(beta-amino ester)s with uniformly distributed branching units. *J. Controlled Release* **2024**, *367*, 197−208.
(11) Gao, X.; Dong, D.; Zhang, C.; Deng, Y.; Ding, J.; Niu, S.; Tan, S.; Sun, L. Chitosan-Functionalized Poly(beta-Amino Ester) Hybrid System for Gene Delivery in Vaginal Mucosal Epithelial Cells. *Pharmaceutics* **2024**, *16* (1), 154.
(12) Dosta, P.; Tamargo, I.; Ramos, V.; Kumar, S.; Kang, D. W.; Borros, S.; Jo, H. Delivery of Anti-microRNA-712 to Inflamed Endothelial Cells Using Poly(beta-amino ester) Nanoparticles Conjugated with VCAM-1 Targeting Peptide. *Adv. Healthc Mater.* **2021**, *10* (15), No. e2001894.
(13) Rodriguez, M.; Soler, Y.; Muthu Karuppan, M. K.; Zhao, Y.; Batrakova, E. V.; El-Hage, N. Targeting Beclin1 as an Adjunctive Therapy against HIV Using Mannosylated Polyethylenimine Nanoparticles. *Pharmaceutics* **2021**, *13* (2), 223.
(14) Patnaik, S.; Gupta, K. C. Novel polyethylenimine-derived nanoparticles for in vivo gene delivery. *Expert Opin Drug Deliv* **2013**, *10* (2), 215−28.
(15) Urban-Klein, B.; Werth, S.; Abuharbeid, S.; Czubayko, F.; Aigner, A. RNAi-mediated gene-targeting through systemic application of polyethylenimine (PEI)-complexed siRNA in vivo. *Gene Ther.* **2005**, *12* (5), 461−6.
(16) Ragelle, H.; Vandermeulen, G.; Préat, V. Chitosan-based siRNA delivery systems. *J. Controlled Release* **2013**, *172* (1), 207−218.
(17) Karlsson, J.; Rhodes, K. R.; Green, J. J.; Tzeng, S. Y. Poly(beta-amino ester)s as gene delivery vehicles: challenges and opportunities. *Expert Opin Drug Deliv* **2020**, *17* (10), 1395−1410.
(18) Lynn, D. M.; Langer, R. Degradable Poly(*β*-amino Esters): Synthesis, Characterization, and Self-Assembly with Plasmid DNA. *J. Am. Chem. Soc.* **2000**, *122* (44), 10761−10768.
(19) Akinc, A.; Lynn, D. M.; Anderson, D. G.; Langer, R. Parallel synthesis and biophysical characterization of a degradable polymer library for gene delivery. *J. Am. Chem. Soc.* **2003**, *125* (18), 5316−23.
(20) Eltoukhy, A. A.; Chen, D.; Alabi, C. A.; Langer, R.; Anderson, D. G. Degradable terpolymers with alkyl side chains demonstrate enhanced gene delivery potency and nanoparticle stability. *Adv. Mater.* **2013**, *25* (10), 1487−93.
(21) Jin, Y.; Wang, X.; Kromer, A. P. E.; Müller, J. T.; Zimmermann, C.; Xu, Z.; Hartschuh, A.; Adams, F.; Merkel, O. M. Role of Hydrophobic Modification in Spermine-Based Poly(*β*-amino ester)s for siRNA Delivery and Their Spray-Dried Powders for Inhalation and Improved Storage. *Biomacromolecules* **2024**, *25* (7), 4177−4191.
(22) Winkeljann, B.; Keul, D. C.; Merkel, O. M. Engineering poly- and micelleplexes for nucleic acid delivery - A reflection on their endosomal escape. *J. Controlled Release* **2023**, *353*, 518−534.
(23) Bruininks, B. M.; Souza, P. C.; Ingolfsson, H.; Marrink, S. J. A molecular view on the escape of lipoplexed DNA from the endosome. *Elife* **2020**, *9*, e52012.
(24) Grimme, C. J.; Hanson, M. G.; Corcoran, L. G.; Reineke, T. M. Polycation Architecture Affects Complexation and Delivery of Short Antisense Oligonucleotides: Micelleplexes Outperform Polyplexes. *Biomacromolecules* **2022**, *23* (8), 3257−3271.
(25) Holzerny, P.; Ajdini, B.; Heusermann, W.; Bruno, K.; Schuleit, M.; Meinel, L.; Keller, M. Biophysical properties of chitosan/siRNA polyplexes: profiling the polymer/siRNA interactions and bioactivity. *J. Controlled Release* **2012**, *157* (2), 297−304.
(26) Li, Y.; He, Z.; A, S.; Wang, X.; Li, Z.; Johnson, M.; Foley, R.; Saez, I. L.; Lyu, J.; Wang, W. Artificial Intelligence (AI)-Aided Structure Optimization for Enhanced Gene Delivery: The Effect of the Polymer Component Distribution (PCD). *ACS Appl. Mater. Interfaces* **2023**, *15* (30), 36667−36675.
(27) Binder, J.; Winkeljann, J.; Steinegger, K.; Trnovec, L.; Orekhova, D.; Zahringer, J.; Horner, A.; Fell, V.; Tinnefeld, P.; Winkeljann, B.; Friess, W.; Merkel, O. M. Closing the Gap between Experiment and Simulation horizontal line A Holistic Study on the Complexation of Small Interfering RNAs with Polyethylenimine. *Mol. Pharmaceutics* **2024**, *21* (5), 2163−2175.
(28) Ouyang, D.; Zhang, H.; Herten, D. P.; Parekh, H. S.; Smith, S. C. Structure, dynamics, and energetics of siRNA-cationic vector complexation: a molecular dynamics study. *J. Phys. Chem. B* **2010**, *114* (28), 9220−30.
(29) Marquet, F.; Stojceski, F.; Grasso, G.; Patrulea, V.; Danani, A.; Borchard, G. Characterization of the Interaction of Polymeric Micelles with siRNA: A Combined Experimental and Molecular Dynamics Study. *Polymers (Basel)* **2022**, *14* (20), 4409.
(30) Bono, N.; Coloma Smith, B.; Moreschi, F.; Redaelli, A.; Gautieri, A.; Candiani, G. In silico prediction of the in vitro behavior of polymeric gene delivery vectors. *Nanoscale* **2021**, *13* (17), 8333−8342.
(31) Paloncyova, M.; Srejber, M.; Cechova, P.; Kuhrova, P.; Zaoral, F.; Otyepka, M. Atomistic Insights into Organization of RNA-Loaded Lipid Nanoparticles. *J. Phys. Chem. B* **2023**, *127* (5), 1158−1166.
(32) Souza, P. C. T.; Alessandri, R.; Barnoud, J.; Thallmair, S.; Faustino, I.; Grunewald, F.; Patmanidis, I.; Abdizadeh, H.; Bruininks, B. M. H.; Wassenaar, T. A.; Kroon, P. C.; Melcr, J.; Nieto, V.; Corradi, V.; Khan, H. M.; Domanski, J.; Javanainen, M.; Martinez-Seara, H.; Reuter, N.; Best, R. B.; Vattulainen, I.; Monticelli, L.; Periole, X.; Tieleman, D. P.; de Vries, A. H.; Marrink, S. J. Martini 3: a general purpose force field for coarse-grained molecular dynamics. *Nat. Methods* **2021**, *18* (4), 382−388.
(33) Li, Z.; Guo, R.; Zhang, Z.; Yong, H.; Guo, L.; Chen, Z.; Huang, D.; Zhou, D. Enhancing gene transfection of poly(beta-amino ester)s through modulation of amphiphilicity and chain sequence. *J. Controlled Release* **2024**, *368*, 131−139.
(34) Zhao, X.; Xu, Q.; Wang, Q.; Liang, X.; Wang, J.; Jin, H.; Man, Y.; Guo, D.; Gao, F.; Tang, X. Induced Self-Assembly of Vitamin E-Spermine/siRNA Nanocomplexes via Spermine/Helix Groove-Specific Interaction for Efficient siRNA Delivery and Antitumor Therapy. *Adv. Healthc Mater.* **2024**, *13*, No. e2303186.
(35) Claveras Cabezudo, A.; Athanasiou, C.; Tsengenes, A.; Wade, R. C. Scaling Protein-Water Interactions in the Martini 3 Coarse-Grained Force Field to Simulate Transmembrane Helix Dimers in Different Lipid Environments. *J. Chem. Theory Comput* **2023**, *19* (7), 2109−2119.
(36) Boeckle, S.; von Gersdorff, K.; van der Piepen, S.; Culmsee, C.; Wagner, E.; Ogris, M. Purification of polyethylenimine polyplexes highlights the role of free polycations in gene transfer. *J. Gene Med.* **2004**, *6* (10), 1102−11.
(37) Jin, Y.; Adams, F.; Nguyen, A.; Sturm, S.; Carnerio, S.; Muller-Caspary, K.; Merkel, O. M. Synthesis and application of spermine-based amphiphilic poly(beta-amino ester)s for siRNA delivery. *Nanoscale Adv.* **2023**, *5* (19), 5256−5262.
(38) Gary, D. J.; Min, J.; Kim, Y.; Park, K.; Won, Y. Y. The Effect of N/P Ratio on the In Vitro and In Vivo Interaction Properties of PEGylated Poly[2-(dimethylamino)ethyl methacrylate]-Based siRNA Complexes. *Macromol. Biosci.* **2013**, *13* (8), 1059−1071.
(39) Wang, X.; Kelkar, S. S.; Hudson, A. G.; Moore, R. B.; Reineke, T. M.; Madsen, L. A. Quantitation of Complexed versus Free Polymers in Interpolyelectrolyte Polyplex Formulations. *ACS Macro Lett.* **2013**, *2* (11), 1038−1041.
(40) Kluenker, M.; Mondeshki, M.; Nawaz Tahir, M.; Tremel, W. Monitoring Thiol-Ligand Exchange on Au Nanoparticle Surfaces. *Langmuir* **2018**, *34* (4), 1700−1710.

https://doi.org/10.1021/acs.nanolett.4c04291
Nano Lett. 2024, 24, 15683−15692

(41) Keniry, M. A.; Owen, E. A. Insight into the molecular recognition of spermine by DNA quadruplexes from an NMR study of the association of spermine with the thrombin-binding aptamer. *Journal of Molecular Recognition* **2013**, *26* (7), 308−317.
(42) Perrin, C. L.; Dwyer, T. J. Application of two-dimensional NMR to kinetics of chemical exchange. *Chem. Rev.* **1990**, *90* (6), 935−967.
(43) Kumar, A.; Ernst, R. R.; Wuthrich, K. A two-dimensional nuclear Overhauser enhancement (2D NOE) experiment for the elucidation of complete proton-proton cross-relaxation networks in biological macromolecules. *Biochem. Biophys. Res. Commun.* **1980**, *95* (1), 1−6.
(44) Levitt, M. H. *Spin Dynamics: Basics of Nuclear Magnetic Resonance*, 2nd ed.; Wiley, 2008.
(45) de Jong, D. H.; Baoukina, S.; Ingólfsson, H. I.; Marrink, S. J. Martini straight: Boosting performance using a shorter cutoff and GPUs. *Comput. Phys. Commun.* **2016**, *199*, 1−7.
(46) Sagui, C.; Darden, T. A. Molecular Dynamics Simulations of Biomolecules: Long-Range Electrostatic Effects. *Annu. Rev. Biophys. Biomol. Struct.* **1999**, *28* (1), 155−179.
(47) Coelho, F.; Botelho, C.; Paris, J. L.; Marques, E. F.; Silva, B. F. B. Influence of the media ionic strength on the formation and in vitro biological performance of polycation-DNA complexes. *J. Mol. Liq.* **2021**, *344*, 117930.
(48) Lou, B.; Connor, K.; Sweeney, K.; Miller, I. S.; O'Farrell, A.; Ruiz-Hernandez, E.; Murray, D. M.; Duffy, G. P.; Wolfe, A.; Mastrobattista, E.; Byrne, A. T.; Hennink, W. E. RGD-decorated cholesterol stabilized polyplexes for targeted siRNA delivery to glioblastoma cells. *Drug Deliv Transl Res.* **2019**, *9* (3), 679−693.
(49) Gessner, A.; Lieske, A.; Paulke, B.; Muller, R. Influence of surface charge density on protein adsorption on polymeric nanoparticles: analysis by two-dimensional electrophoresis. *Eur. J. Pharm. Biopharm* **2002**, *54* (2), 165−70.
(50) Vermeulen, L. M. P.; De Smedt, S. C.; Remaut, K.; Braeckmans, K. The proton sponge hypothesis: Fable or fact? *Eur. J. Pharm. Biopharm* **2018**, *129*, 184−190.
(51) Benjaminsen, R. V.; Mattebjerg, M. A.; Henriksen, J. R.; Moghimi, S. M.; Andresen, T. L. The possible ″proton sponge ″ effect of polyethylenimine (PEI) does not include change in lysosomal pH. *Mol. Ther* **2013**, *21* (1), 149−57.
(52) Hartl, N.; Jurgens, D. C.; Carneiro, S.; Konig, A. C.; Xiao, X.; Liu, R.; Hauck, S. M.; Merkel, O. M. Protein corona investigations of polyplexes with varying hydrophobicity - From method development to in vitro studies. *Int. J. Pharm.* **2023**, *643*, 123257.
(53) Dosta, P.; Segovia, N.; Cascante, A.; Ramos, V.; Borrós, S. Surface charge tunability as a powerful strategy to control electrostatic interaction for high efficiency silencing, using tailored oligopeptide-modified poly(beta-amino ester)s (PBAEs). *Acta Biomaterialia* **2015**, *20*, 82−93.
(54) Shi, J.; Choi, J. L.; Chou, B.; Johnson, R. N.; Schellinger, J. G.; Pun, S. H. Effect of Polyplex Morphology on Cellular Uptake, Intracellular Trafficking, and Transgene Expression. *ACS Nano* **2013**, *7* (12), 10612−10620.
(55) Stevens, J. A.; Grunewald, F.; van Tilburg, P. A. M.; Konig, M.; Gilbert, B. R.; Brier, T. A.; Thornburg, Z. R.; Luthey-Schulten, Z.; Marrink, S. J. Molecular dynamics simulation of an entire cell. *Front Chem.* **2023**, *11*, 1106495.

https://doi.org/10.1021/acs.nanolett.4c04291
Nano Lett. 2024, 24, 15683−15692